MAPPING HAZARDS WITH MICROSEISMIC TECHNOLOGY TO ANTICIPATE ROOF FALLS - A CASE STUDY

Anthony T. Iannacchione, *Senior Scientist*
Timothy Batchler, *Mechanical Engineer*
Thomas E. Marshall, *Engineering Technician*
National Institute for Occupational Safety and Health
Pittsburgh Research Laboratory
Pittsburgh, Pennsylvania USA

ABSTRACT

As the amount of new fractured surfaces or "damaged rock layers" within roof rock increases, the stability of the rock mass decreases. While direct measurements of this phenomenon are not easily made, there is good circumstantial evidence to support this hypothesis. For example, it is common to observe increased cracks or fractures in the immediate mine roof rock before a roof fall. Likewise, roof drill holes placed in areas that later fail often reveal increased numbers and/or separations of fractures within the rock column through time. And finally, the frequency of microseismic activity, representative of rock fracturing, increases before a roof fall.

For this study, more than 700 microseismic emissions were collected from two underground limestone mine roof fall areas in southwestern Pennsylvania. Microseismic events were located and magnitudes determined using the moment magnitude technique. Moment magnitude is based on the event seismic moment, which is a measure of the seismic deformation. The amount of new fracture surface length was calculated based on the stored strain energy within the rock prior to fracture. In the two case studies presented, a significant amount of microseismic activity was observed as much as two days before the first signs of failure in the roof fall areas. Additionally, results from this analysis reveal much about the behavior of strata prone to failure and allows for the construction of hazard maps based on microseismic emissions. The potential use of this technique as a means of anticipating roof falls is analyzed and discussed.

INTRODUCTION

For years, the international mining safety research community has attempted to develop technology that will provide warning of impending roof falls. Many different methods and techniques have been tried with varying degrees of success. A significant hindrance to applying roof fall warning techniques is the lack of knowledge concerning the behavior of pre-fall rock strata and their associated precursor characteristics. It is difficult to apply any technology if our basic understanding of the important characteristics of the phenomenon are unknown. Therefore, a key requirement is to determine the rock failure processes leading to a roof fall. It is also important to recognize that these pre-rock fall behaviors will depend on site specific conditions, such as geology, in situ stress, and mine layout.

The use of microseismic activity to warn of roof falls was first evaluated in the 1940's (Obert and Duvall, 1945a & 1945b) for monitoring general stability conditions. Later, Leighton and Stebley (1977) demonstrated that increased noise rates, from a system capturing events in the 36 to 44 kHz range, preceded the failure of a coal mine roof by as much as 15 minutes. They recorded ultrasonic signals because excessive amounts of cultural noise existed in the lower frequency ranges. Unfortunately, the ultrasonic frequencies attenuate rapidly, requiring geophones placement within 40 m of the roof fall events. These kinds of system requirements present numerous operational issues. Ideally, roof fall warning systems need to be capable of monitoring large areas of the mine with a minimal number of geophones.

Since this early work, much of the mining induced seismicity research has been focused on the rock burst, coal bump, and gas outburst problems. This focus on dynamic failures has produced analysis techniques that can be traced to earthquake seismology. Analytical procedures that rely on techniques developed for earthquake seismology to determine the magnitude and energy associated with rock failure events are ill equipped for the roof fall problem. Earthquakes are typically associated with fault planes with large rupture surfaces and comparatively small displacements. Events leading to roof falls are comprised of many small releases of energy that represent shear and tensile failure both through intact rock and along preexisting discontinuities in the rock. It is assumed that the rock stress drop is complete since the roof beams fail next to the mine opening, virtually eliminating any confining stress. Also, the rupture surfaces are typically much smaller than the width of the mine openings (<14 m). Therefore, roof fall analyses need to focus on smaller rock failure events with high source area stress drops and small rupture surfaces.

Gale (2003) proposed a technique to overcome this discrepancy by calculating the amount of new rock fracture length generated from each pre-roof fall seismic event. Defining roof stability based on this parameter has a well defined meaning. It also allowed for the summation of lengths so that the accumulation of damage can be tracked through time. Tracking the time and location of new rock fracture surfaces allows for the construction of isopach maps that display the intensity of new fractured ground within a wide mining area. These intensity data are then used to construct hazard maps. The effectiveness of these maps in warning of actual roof fall conditions at two different sites is assessed in this study.

Study Site Conditions

Hazard mapping with microseismic activity was attempted at a room-and-pillar underground limestone mine with rooms 14 m wide and 9 m high (figure 1). The microseismic system had originally been installed at this site to evaluate different mine layouts used to control hazards associated with roof falls (Iannacchione et al., 2003). The unit mined is the Loyalhanna Limestone, a very strong rock unit with unconfined compressive strengths as high as 210 MPa. Locally, the Loyalhanna ranges from 15 to 21 m thick with dips between 1 to 7°. The rock mass characteristics of this unit consist of horizontal bedding planes spaced from 1 to 1.5 m apart, widely spaced vertical joints, and extensive cross bedding within the individual rock layers (Iannacchione and Coyle, 2002). The Loyalhanna is overlain by weak Mauch Chunk shales and siltstones. Approximately 300 m from the study area and under 120 m of overburden, high horizontal stresses were measured, reaching a maximum value of approximately 55 MPa in the N 60° E orientation (Iannacchione and Coyle, 2002). These factors are important because the behavior of this roof rock is dominated by stiff, relatively thin rock layers, subjected to excessive levels of horizontal stress.

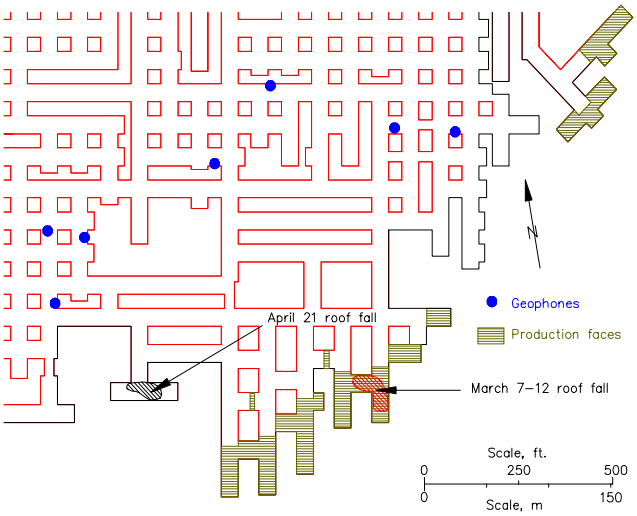

Figure 1. Mine map showing the location of the area monitored by the microseismic network. Also shown are the locations of the geophones, the faces mined from November 1, 2001 to April 21, 2002, and the March 7 and April 21 roof falls.

As part of this research, 15 4.5-Hz 630-ohm uniaxial geophones were connected to a microseismic system. All but one of the geophones were mounted on the roof about 10 m above the mine floor. One geophone was placed 21 m beneath the mine floor within a borehole. The heights of the events above the mine roof could not be determined because almost all geophones were located within the same horizontal plane. Data collected included dates and locations of roof falls and face advances (figure 1).

TWO DISTINCT ROOF FALL AREAS

Two major roof fall episodes occurred during this study. Each of these episodes was comprised of one to several individual roof falls that either fell suddenly as one mass or gradually as many smaller rock falls over distinct time intervals from a few minutes to many hours. The March 7 roof fall occurred in the southeast corner of the mine while April 21 roof fall occurred approximately 150 m to the west-northwest (figure 1). From November 1, 2001 to April 21, 2002, 92 face cuts were advanced by blasting in the study area (figure 1).

The first sign of failure associated with the March 7 roof fall occurred when mine officials noticed a shear failure in the immediate roof around 3 am. By that afternoon, a small shallow fall extended approximately 0.6 m into the roof. Sometime during the evening of March 7 the roof fall cavity extended across the intersection and approximately 3 m into the roof, encountering the soft red shales of the Mauch Chunk Formation. From late March 10 into the morning of March 11, the roof fall extended to the southeast where it was stopped by the unmined limestone perimeter. During the morning of March 12, the roof fall extended to the northwest, causing the roof bolts to fail in tension followed by the collapse of a large section of roof. Figure 1 shows the total area of the roof fall developed between March 7-12. Small rocks continued to dribble from the roof fall until March 14. The roof fall cavity created during this period extended over 38 m in length and up to 6 m in height (figure 2a). After the March 14 event, the area around the roof fall stabilized for a period of approximately two months.

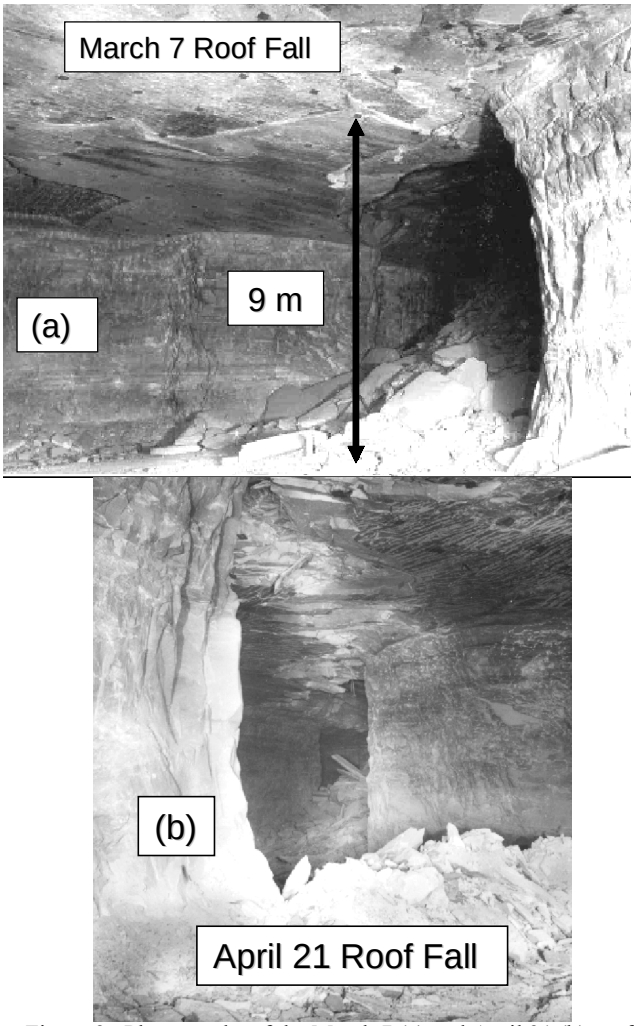

Figure 2. Photographs of the March 7 (a) and April 21 (b) roof falls.

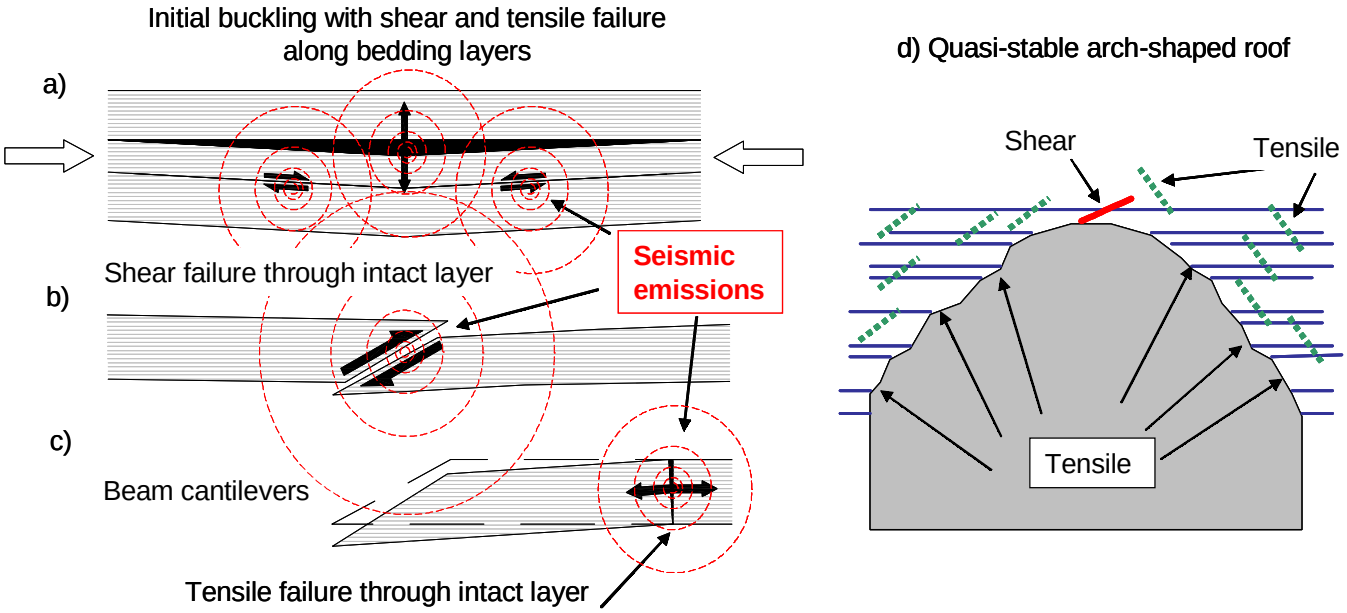

Figure 3. Generalized sequence in which individual roof beams fail and develop into large roof falls.

The April 21 roof fall was initiated with a single roof slab fall around 8 am which eventually developed into a shallow roof fall that encompassed the entire intersection (figure 2b). This area had experienced some roof rock fracturing within the past year but had been relatively stable for several months. About two weeks after the April 21 roof fall, a series of instabilities occurred that resulted in several northerly roof fall extensions.

ROOF FALL CHARACTERISTICS

Rock failures in bedded formations with excessive levels of horizontal stress can be initiated when the stiffest and thinnest beds in the roof strata begin to buckle from the horizontal loading (figure 3a). When these layers buckle, shear and tensile rupture between layers and low-angle shears through the intact rock layers can occur (figure 3b). Eventually the beam begins to cantilever, initiating a tensile failure along the fixed contact area at the edge of the roof fall (figure 3c). One-by-one the individual roof beams are strained to failure, shedding their load to adjacent layers which are also strained to failure. In the end, the shape of the roof cavity is defined by the sub-vertical tensile failures (figure 3d). Quasi-stable conditions are achieved as the roof takes on the more stable arched shape.

Sometimes these falls remain active at their axial ends where the stress concentrations are the highest. There also seems to be a slow, methodical de-stabilization of roof beams in the very highest sections of the roof fall. Experience has shown that roof falls can slowly expand upward over the course of many years.

Roof falls at the study site, are typically 14 m wide by 8 m high and extend up to 150 m in length. A single roof fall could easily be associated with several hundred shear and tensile seismic events that are detectable with a microseismic system similar to the one used in this study. The amount of seismic energy released by these rock fracture events is dependent upon the size of the fracture, the characteristics of the in situ rock unit, the pre-failure state of stress, and the mode of failure (shear vs. tension). Because the latter three characteristics are unknown, it is assumed that the size of the event is largely dependent on the size of the new fracture surface.

The smaller fractures require more geophones at locations closer to the source events. In the study area, 15 geophones had been deployed in an asymmetric pattern. The geophones closest to the two roof falls were more than 75 m from these areas. Many of the smallest seismic emissions associated with the rock fractures were below the detection threshold of the system. Therefore the source of the activity recorded at the study site primarily represents only the larger events emanating from the roof fall areas.

SIZE OF MICROSEISMIC EVENTS

Analysis capabilities are limited when the event magnitude is unknown. Characterization of event magnitude allows for interpretation of subtle relationships that are not possible with data limited to time and location. Moment magnitude (M) is a technique used by many international researchers and technicians to determine the size of microseismic events. The moment magnitude is based on its seismic moment (M_o).

Moment magnitude (Hanks and Kanamori, 1979) is based on the static seismic moment by the relationship:

$$M = (2/3) \cdot \log_{10}(M_o) - 6.0, \quad (1)$$

where M_o is expressed in SI units (N-m). The seismic moment (Aki, 1968) is determined from the observed Fourier displacement amplitude spectrum of body waves, the density of the rock at the source, the P wave velocity, the distance between source and receiver, and P wave radiation pattern coefficient for source and receiver. Seismic moment is a measure of deformation. Seismic moments and moment magnitudes were determined for 715 microseismic events reported on in this study.

The radiated seismic energy, E_s (Boatwright and Fletcher, 1984), another measure of the seismic source, is determined from the radiation pattern coefficient for P or S waves, the integral of the squared velocity for P or S wave motion, the density of the rock at the source, the S wave velocity, and the distance between source and receiver. Seismic energy values were determined with the Engineering Seismology Group Canada, Inc. (ESG) microseismic

analysis software program (Anon, 2002). From November 1, 2001 until April 21, 2002 the seismic moment ranged from 3.73E+5 N-m to 1.04E+9 N-m while the seismic energy ranged from 0.01 to 174 Joules. The seismic moment and seismic energy typically are linearly related (figure 4). Variations in the data are attributed to the seismic moment using only the P wave portion of the signature, while seismic energy calculations uses the entire signature.

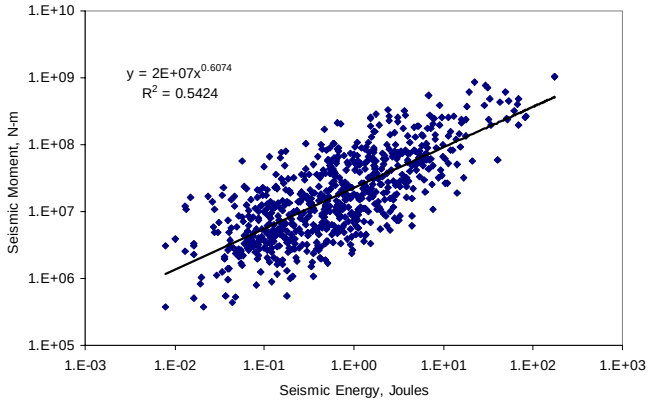

Figure 4. Relationship between the seismic moment and seismic energy for each of the 715 events used in this study.

MOMENT MAGNITUDE VARIATIONS

Moment magnitude values of events from November, 2001 until April 21, 2002 are shown in figure 5. The events range from approximately -2.29 to 0.01 with an average value of -1.18. The data shows definitive event clustering in association with the March 7 and April 21 roof falls. It is also evident that a relatively steady rate of background seismicity occurs between these two roof fall events. This data indicate that increased microseismic activity only started two days prior to the March 7 roof fall. Additionally, there is some evidence that the overall magnitude of events drops slightly after the March 7 roof fall episode.

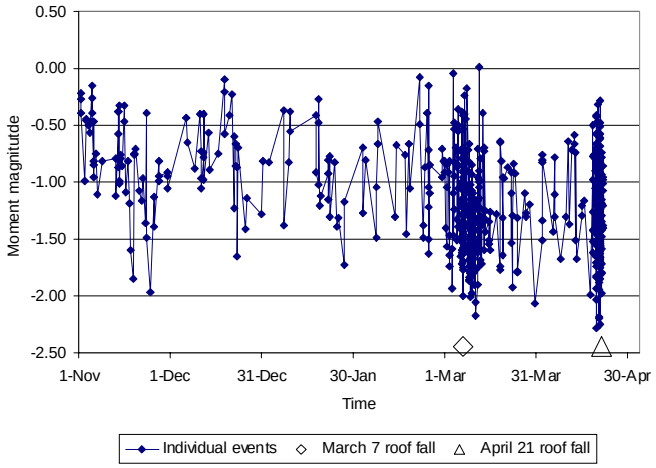

Figure 5. Variation in moment magnitudes for the 715 events from November 1, 2001 to April 21, 2002.

The locations of the microseismic events were entirely within the area shown in figure 1. Most of the events were within 100 m of the center of either the March 7 and April 21 roof fall episodes. Often the largest events were within 30 m of the roof falls. In contrast, many of the microseismic events occurring away from the fall areas were comparatively small.

TECHNIQUE FOR DETERMINING NEW ROCK FRACTURE LENGTH

In this study, the seismic energy for each event has been measured and the corresponding new fracture length calculated. This methodology is utilized to provide the mine operator and worker with a more useable and effective means of interpreting microseismic data. Miners can relate to the amount of new fractured rock developed in the roof above their heads. Gale (2003) determined an energy release method based on the stored strain energy within the rock before fracture. According to Hatherly, et al. (2003) this method is in line with current rock mechanics principles. Gale derived equation 2 for determining energy release from shear through intact rock:

$$\text{Energy(shear failure)} = Lf^3 * \Delta\tau xy^2 \ / (2*G) \text{ [units of N·m]} \quad (2)$$

where:

$\Delta\tau xy$ = Shear stress drop ~ Unconfined compressive strength/2
Lf = Length of fracture, m
G = Shear modulus = (S wave velocity)^2 x density

Because shear through intact rock produces the most energy, equation 2 probably represents the source mechanism associated with the majority of the events detected by the NIOSH microseismic system. The shape of the shear rupture surface is assumed to be square.

Core was recovered from a nearby mine in the Loyalhanna Limestone and tested at NIOSH's Pittsburgh Research Laboratory. Eleven NX size cores produced an average uniaxial unconfined compression strength of 136.4 MPa. This yielded an estimated $\Delta\tau xy$ value of 68.2 MPa. While Gale suggested using the shear modulus calculated from Young's modulus and Poisson's ratio, this study used the shear modulus from available S wave velocity data. The shear modulus of 1.65 x 10^4 MPa is calculated from a shear wave velocity of 2,574 m/s and a density of 2,500 kg-m/s.

Through a derivation of the above formulas, the length of new fractures formed as a result of both shear and tensile failure can be calculated:

$$Lf\,(\text{shear failure}) = \sqrt[3]{(\text{Energy} * (2 * G)) / \Delta\tau xy^2} \quad (3)$$

The energy used in this equation comes from seismic energy calculations discussed earlier. McGarr (1999) has indicated that the maximum seismic efficiency for earthquakes is less than 6%. Event energy was calculated by dividing the seismic energy by a seismic efficiency of 4%. In this way, equation 3 was used to estimate the length of new fracture lengths produced by each microseismic event.

NEW FRACTURE LENGTH ESTIMATES AND PRECURSOR ROOF FALL PATTERNS

Calculations of the new fracture lengths produced between November 1, 2001 and April 21, 2002 in the study area are shown in figure 6. Approximately 41 m of new fractures were developed during this time. Almost 15 m of these new fracture lengths were developed between March 6 and 12 and approximately 12 m between April 19 and 21. After the initial March 7-12 roof fall, the rate of new fracture development was reduced to pre-March 7 roof fall values.

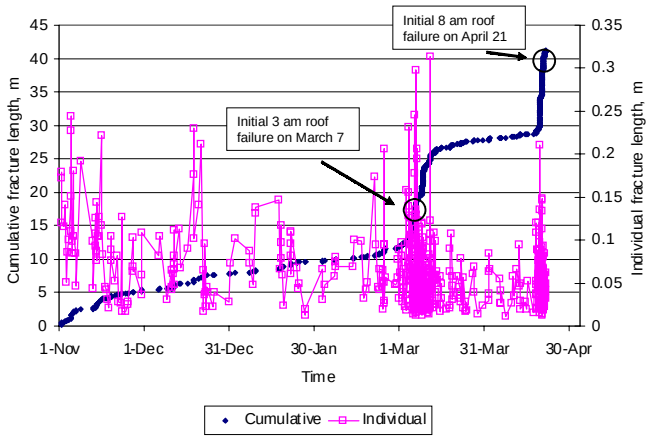

Figure 6. Graph displays both the individual and cumulative new fracture lengths generated from November 1, 2001 to April 21, 2002.

What is of most interest to this study is the character of the pre-fall microseismic activity. Figure 7a shows activity before and after 3 am on March 7 when the first visible sign of failure occurred with a shear crack and a small rock fall. By the afternoon of the same day, a small section of roof, approximately 0.6 m deep, extended into the roof. Figure 7a shows a moderately intense period of microseismic activity starting around 2 am and gradually declining until 8 am. More importantly, another moderately intense period of microseismic activity occurred at 5 pm on March 6, some 10 hours before the first recognition of the unstable roof rock conditions. It is also interesting to note that the period between 6:30 pm on March 6 and 2 am on March 7, prior to the roof fall, was marked by very low microseismic activity.

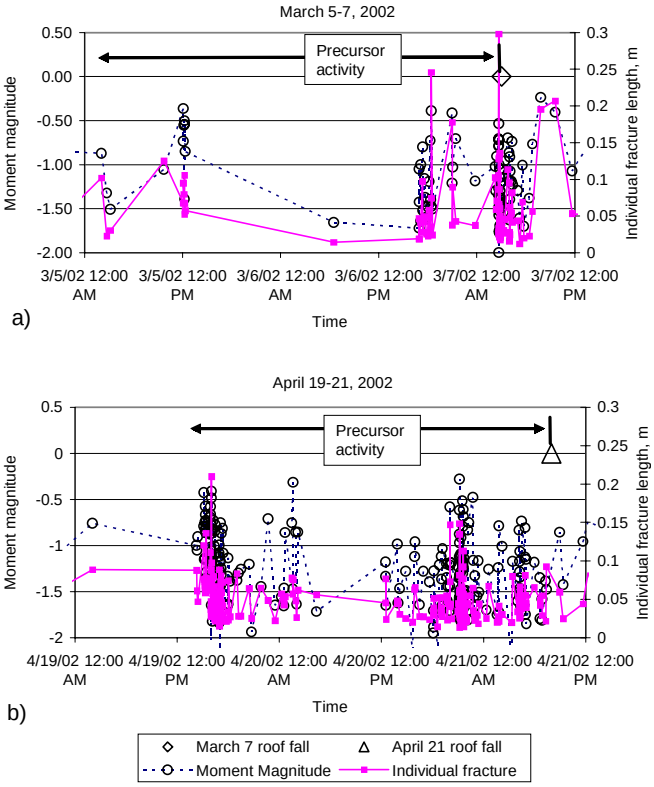

Figure 7. Moment magnitudes and new fracture lengths for microseismic events that occurred 2 days prior to the March 7 (a) and April 21 (b) roof falls.

Figure 7b shows activity before and after 8 am on April 21 when a slab of rock fell from the roof, signaling the beginning of that roof fall. An intense spike lasting approximately 2 hours in duration occurred 41 hours before the start of the roof fall. This was followed by approximately 8 hours of moderate activity which was in-turn followed by approximately 10 hours of quiet. Activity increased again around noon on April 20 and continued at a fairly constant rate through the initiation of the roof fall some 20 hours later.

CONSTRUCTING HAZARD MAPS

The data presented indicate that an increased level of microseismic activity occurred before the first recognition of roof failure at 3 am on March 7 and 8 am on April 21. How does the location of this activity relate to the roof fall events? If all events were of equal magnitude, a simple two-dimensional plot of event locations would suffice. However, as previously demonstrated, rock fracturing events have significant variation in magnitude. Typically, the event size would be represented by a symbol scaled to the moment magnitude of the microseismic event. From November 1, 2001 to March 5, 2002 at 3 am, some 48 hours before the first signs of failure in association with the March 7 roof fall, 166 microseismic events occurred within the study area. During this time microseismic events in the study area appear to be occurring in a fairly random fashion. There was no evidence of the impending roof fall from the microseismic information.

The trend changes dramatically at approximately 12 noon on March 5. Sixty-two microseismic events occurred in the 48 hour period before the first sign of failure in association with the March 7 roof fall. These events tend to cluster around the March 7 roof fall producing approximately 3.9 m of new fracture lengths.

The study area was divided into 30.5 m squares and all the new fracture lengths found in each square were added together. The sum of all new fracture lengths for each zone was used to construct an isopach map for the March 7 roof fall (figure 8). In general, the zones surrounding the March 7 roof fall tend to have total fracture lengths of greater than 0.2 m with many greater than 0.4 m.

A similar analysis was performed for the April 21 roof fall episode. Figure 9 shows the combined totals of new fractured rock within 30.5 m squares from 8 am on April 19 until 8 am April 21. This 48 hour interval produced almost 11 m of new fracture length from 217 microseismic events. There is a strong correlation between the intensity of new rock fractures and the location of the April 21 roof fall. The majority of the microseismic events that represented rock fracture development were within 50 m of the roof fall.

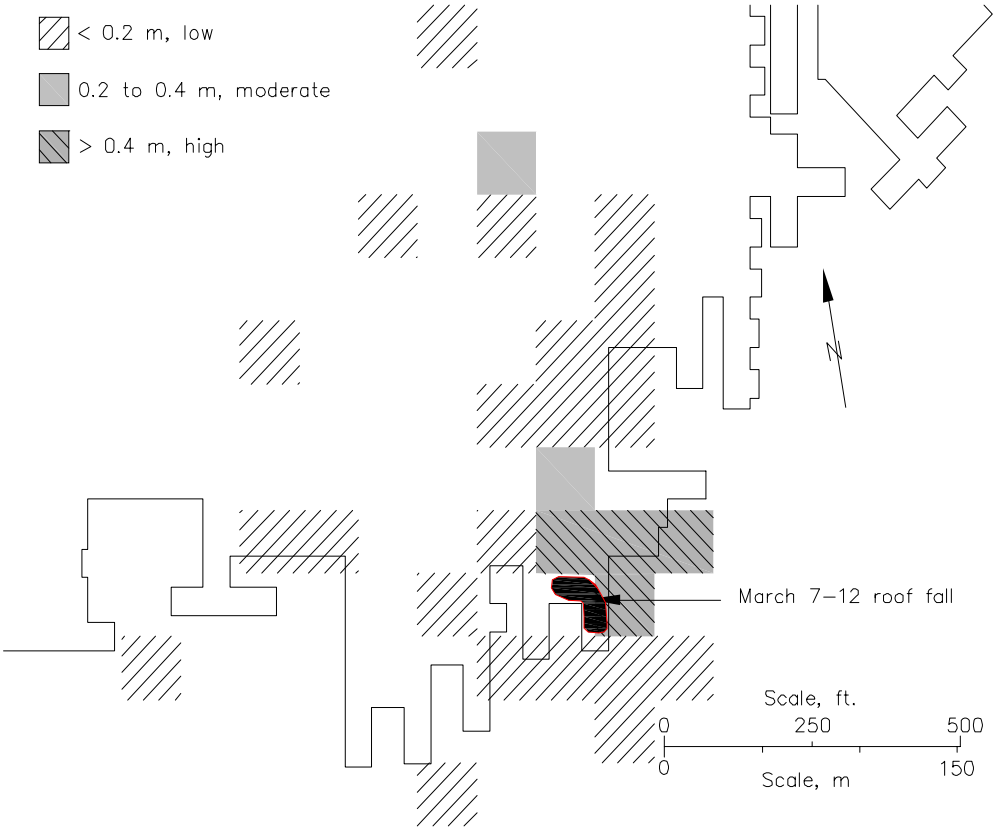

Figure 8. A hazard map containing the total new fracture lengths within 30.5 m square grids within the study area over the 48 hours prior to the March 7 roof fall.

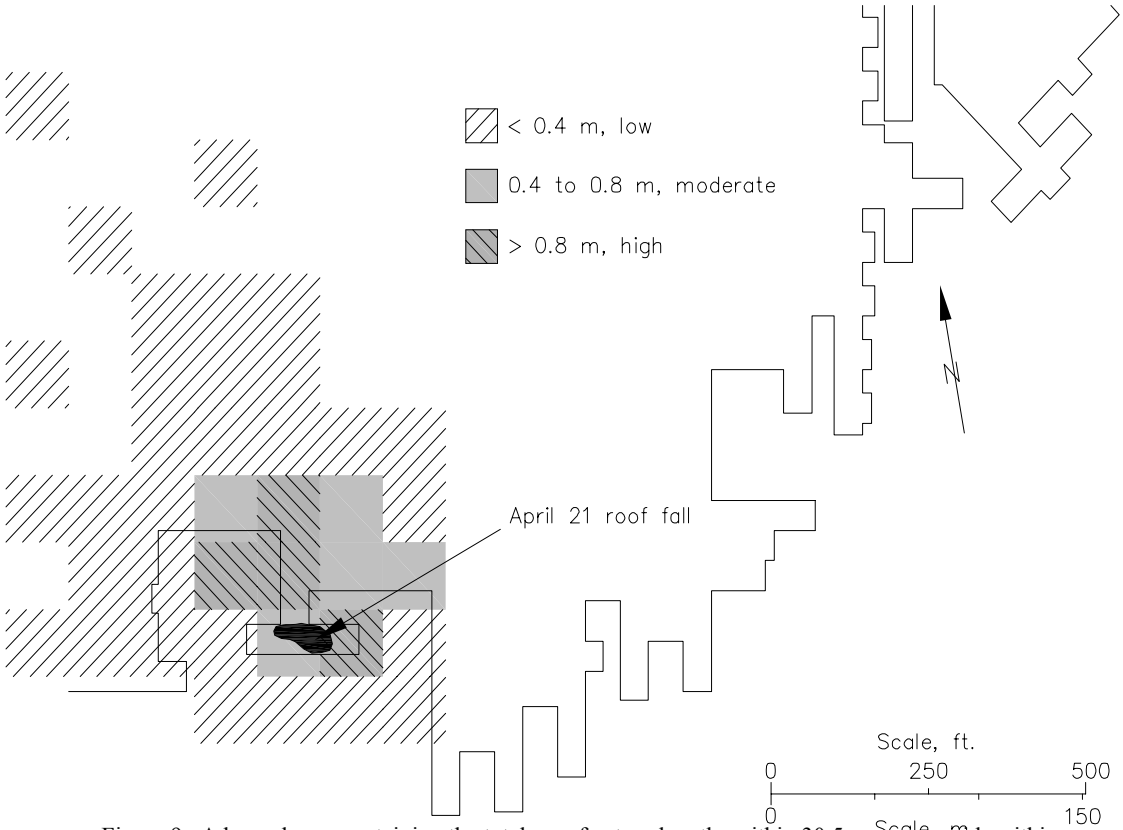

Figure 9. A hazard map containing the total new fracture lengths within 30.5 m square grids within the study area over the 48 hours prior to the April 21 roof fall.

SUMMARY AND CONCLUSIONS

In this study, 715 microseismic signatures were collected and analyzed from an array of 15 geophones to examine failure patterns associated with two large roof falls. In particular, the study determined the appropriateness of constructing hazard maps from microseismic data to warn of impending roof falls. Each event was manually located and its moment magnitude and seismic energy determined. The magnitude of these events ranged between -2.29 and 0.01 with an average of -1.18, while the seismic energies varied between 0.01 and 174 Joules. The lengths of new fracture surfaces were calculated for each event, producing an estimated total of 41 m of new fracture lengths. Most of the new fracture lengths were produced in conjunction with the two roof falls. Of most interest to this study is that 3.9 m of new fracture lengths were produced in the 48 hours prior to the first recognition of failure in association with the March 7 roof fall. Furthermore, the majority of the new fracture surfaces occurred within 100 m of the March 7 roof fall. The April 21 roof fall produced 11 m of new fracture surfaces in the 48 hour period prior to the first signs of roof failure. The majority of these microseismic events were within 50 m of the roof fall.

Because these new fracture lengths are an integral part of roof falls, their detection prior to a roof fall event is crucial for enhancing worker safety. This study shows that for this set of data and under these geologic and mining characteristics, increased levels of microseismic activity occurred within 48 hours of the initial observable rock fall. This microseismic activity is directly related to the failure of individual rock layers which comprise the strata within the zone of roof that will eventually define the roof fall.

Data presented was manually processed, removing all cultural and mining related seismic signatures. This produced event locations and magnitudes that had a high degree of confidence so that accurate new fracture length data could be produced. Real-time application of this technology in the mining industry will require a comprehensive approach to develop systems that accurately and consistently produce fracture length data. There is also a need to calibrate the estimated fracture lengths with laboratory and/or field observations.

The trends established from this case study are dependent on its' unique geology, the state of the mine's stress conditions, and the properties and layout of the microseismic system deployed. It is possible that additional data clarity may have been achieved with a geophone array that completely surrounded the roof fall areas. Unfortunately, limited underground access will make that condition difficult to achieve. It is also possible that the amount of pre-roof fall rock failures may change in intensity and timing with different geologic and stress conditions.

In general, this study demonstrates the potential for this technology to locate future roof fall events in space with, in this case, a high degree of reliability. Determining the exact timing of these events is much more difficult and may prove to be beyond the capabilities of the technology. The data presented, along with recommendations from another NIOSH study (Iannacchione et al., 2004), outline a potential strategy for using monitoring technologies to anticipate, and plan for, roof falls in the underground environment.

REFERENCE

Aki, K. (1968). Seismic Displacements Near a Fault. Journal of Geophysical Research, 73, pp. 5359-5376.

Anon, (2002). Hyperion Seismic System Manual, Engineering Seismology Group, Canada, Inc., p. H-2.

Boatwright, J. and Fletcher. J.B (1984). The Partition of Radiated Seismic Energy Between P and S Waves. Bull. Seism. Soc. Am., 74, pp. 361-376.

Gale, W. (2003). Fracture Mode and Size Related to Microseismic Measurements. In 3D Stress Effects, Rock Damage and Longwall Caving as revealed by Microseismic Monitoring, ed. by Hatherly, Gale, Medhurst, King, Craig, Poulsen and Luo. Report to the Australian Coal Association Research Program, ACARP Project C9012, March, pp. 40-72.

Hanks, T. and Kanamori, H. (1979). A Moment Magnitude Scale. Journal of Geophysical Research, 84, pp. 2348-2350.

Hatherly, P., Gale, W., Medhurst T., King, A., Craig, S., Poulsen, B. and Luo, X. (2003). 3D Stress Effects, Rock Damage and Longwall Caving as Revealed by Microseismic Monitoring. ACARP Project C9021, Exploration and Mining Report 1008F, March, 178 pp.

Iannacchione, A.T. and Coyle, P. (2002). An Examination of the Loyalhanna Limestone's Structural Features and Their Impact on Mining and Ground Control Practices. Proceedings, 21st International Conference on Ground Control in Mining, Morgantown, WV, Aug. 6-8, pp. 218-227.

Iannacchione, A.T., Marshall, T.E., Burke, L.M., Melville, R., and Litsenberger, J. (2003). Safer Mine Layouts for Underground Stone Mines Subjected to Excessive Levels of Horizontal Stress. *Mining Engineering*, April, pp. 25-31.

Iannacchione, A.T., Coyle, P.R., Prosser, L.J., Marshall, T.E. and Litsenberger, J. (2004). The Relationship of Roof Movement and Strata-Induced Microseismic Emissions to Roof Falls. SME Preprint 04-58, SME Annual Meeting, Denver, CO, Feb. 23-25, 9 pp.

Leighton, F. and Steblay. B.J. (1977). Application of Microseismics in Coal Mines. Proceedings, First Conference on Acoustic Emissions/Microseismic Activity in Geologic Structures and Materials, ed. by Hardy and Leighton, Pennsylvania State University, June 9-11, 1975, pp. 205-229.

McGarr, A. (1999). On Relating Apparent Stress to the Stress Causing Earthquake Fault Slip. Journal of Geophysical Research, B, Solid Earth and Planets, Vol. 104, No.2, Feb. 10, pp. 3003-3011.

Obert L. and Duvall, W.I. (1945a). The Microseismic Method of Predicting Rock Failure in Underground Mining, Part 1, General Method. U.S. Bureau of Mines, Report of Investigation 3797, 7 pp.

Obert L. and Duvall, W.I. (1945b). The Microseismic Method of Predicting Rock Failure in Underground Mining, Part 2, Laboratory Experiments. U.S. Bureau of Mines, Report of Investigation 3803, 14 pp.